Worst-Case Response Time of Mixed Vehicles at Complex Intersections

RADHA REDDY [1,4] **(Member, IEEE), LUIS ALMEIDA** [1,3] **(Senior Member, IEEE),**
HARRISON KURUNATHAN[1,2]**, MIGUEL GUTIÉRREZ GAITÁN** [1,5] **(Senior Member, IEEE),**
PEDRO M. SANTOS [1,2,3]**, AND EDUARDO TOVAR** [1,2] **(Member, IEEE)**

[1]CISTER Research Center, 4200-135 Porto, Portugal

[2]Instituto Superior de Engenharia do Porto, 4200-135 Porto, Portugal

[3]Faculdade de Engenharia, Universidade do Porto, 4200-465 Porto, Portugal

[4]Department of Computer Science and Engineering, Amrita School of Computing, Amrita Vishwa Vidyapeetham, Coimbatore 641112, India

[5]Department of Electrical Engineering, Pontificia Universidad Católica de Chile, Santiago 7820436, Chile

CORRESPONDING AUTHOR: R. REDDY (e-mail: reddy@isep.ipp.pt)

ABSTRACT Operating autonomous vehicles (AVs) and human-driven vehicles (HVs) at urban intersections while observing requirements of safety and service level is complex due not only to the existence of multiple inflow and outflow lanes, conflicting crossing zones, and low-speed conditions but also due to differences between control mechanisms of HVs and AVs. Intelligent intersection management (IIM) strategies can tackle the coordination of mixed AV/HV intersections while improving intersection throughput and reducing travel delays and fuel wastage in the average case. An endeavor relevant to traffic planning and safety is assessing whether given worst-case service levels can be met. Given a specific arrival pattern, this can be done via the worst-case response time (WCRT) that any vehicle experiences when crossing intersections. In this research line, this paper estimates WCRT upper bounds and discusses the analytical characterization of arrival and service curves, including estimating maximum queue length and associated worst-case waiting time for various traffic arrival patterns. This analysis is then used to compare six state-of-the-art intersection management approaches from conventional to intelligent and synchronous. The analytical results show the advantage of employing a synchronous management approach and are validated with the vehicles floating car data (timestamped location and speed) and simulations carried out using SUMO.

INDEX TERMS Intelligent intersection management, intelligent transportation systems, mixed traffic, traffic waiting time, urban traffic management.

I. INTRODUCTION

IN RECENT years, the challenge of intersection management (IM) with autonomous vehicles (AVs) has received considerable attention [1], [2], [3], [4], [5], [6]. However, the exclusive presence of AVs on the roads is not expected

The review of this article was arranged by Associate Editor Yajie Zou.

before 2045 [7]. Until then, there will be the need to cope with mixed traffic scenarios composed of AVs and human-driven vehicles (HVs), and specific intelligent intersection management (IIM) protocols are being devised to efficiently handle such scenarios [8], [9], [10], [11]. These works aim to mitigate traffic congestion, improve intersection throughput and fuel efficiency, and reduce travel delays

and air-polluting emissions but focus solely on the average case.

Other less common metrics also relevant for characterizing the performance of such IM strategies are those related to worst-case scenarios [4], [12], [13], [14], [15], [16], [17]. Considering the worst-case situation that can emerge from particular traffic patterns provides useful information for city planners and traffic management entities. It equips them with an estimate of the worst service a given intersection can provide, particularly maximum waiting time and queue size. Knowing the maximum queue size allows tuning the IM configuration to prevent queue spillback at neighboring intersections [12]. In turn, knowing the maximum waiting time is imperative for safety-critical or mission-critical traffic [4], [11], [12], [13], [14], [15], [16], [17].

Our work aims to contribute to this line by characterizing the worst-case service levels provided by several IM options. To this end, we adapt the worst-case response time (WCRT) defined by [15] to a complex multi-lane scenario and consider a wider breadth of IM strategies utilizing arrival-service curves. We introduce the WCRT as an upper bound to the travel delay considering the geometric settings of complex intersections. Knowing the stochastic properties of the traffic arriving at each lane, we produce a deterministic worst-case arrival curve that upper bounds the actual stochastic arrival pattern. The worst-case arrival curve consists of a burst of vehicles arriving under saturation rate, leading to the maximum queue length, followed by a regular arrival of vehicles at the long-term average rate. The worst-case arrival curve together with the service curve of each IM allows for the determination of the WCRT. We apply this analysis to Poisson arrival processes considering various long-term average arrival rates, from low to moderate and saturation traffic conditions. For each situation we use the SUMO simulator [18] to produce the moving vehicles floating car data (FCD), i.e., timestamped vehicle location and associated speed, and we compare the simulation-based results against the analytical formulation and characterization.

The IM strategies that we investigate are two conventional ones, namely Round-Robin (RR) [19] and Trivial Traffic Light Control (TTLC) [20] that were initially designed for HV-only scenarios, three IIM strategies, namely Max-pressure Control Algorithm (MCA) [21], [22] and Q-learning based Traffic Light Control (QTLC) [23] that were initially designed for HV-only scenarios too, and Intelligent Traffic Light Control (ITLC) [2] designed for AV-only scenarios, and finally, an IIM strategy proposed for mixed HV/AV traffic, the Synchronous Intersection Management Protocol (SIMP) [24]. In this paper, we analyze the dedicated left-crossing lane intersection type for its popularity, but without loss of generality. Note that the proposed analysis is applicable to any intersection that uses an IM protocol that can be described with a service curve per lane and for which the traffic arrival can be upper bounded by known arrival curves.

Therefore, the primary contribution of this paper is the WCRT analysis that provides upper bounds for the travel time of vehicles crossing intersections. The other contribution is the comparison of six IM protocols in terms of their WCRTs, using the analysis and simulations.

In this regard, we present the following results:

- The WCRT for a given vehicle in a given crossing lane, i.e., left/straight/right;
- The arrival and service curves of the considered traffic scenarios;
- The maximum queue length estimation and associated waiting time;
- Simulations of traffic scenarios for two maximum speeds representing urban mobility and comparison against the previous analytical results per crossing lane, notably:
  - FCD-based maximum queue length and throughput results;
  - FCD-based vehicle queue joining time, intersection service time, and response time for 1000 mixed vehicles at non-saturation traffic flow conditions;
  - Response time and WCRT for saturation traffic flow conditions.

The rest of the paper is organized as follows. The relevant related works are reviewed in Section II. Section III presents the system model, problem statement, and comparing IM protocols. Section IV introduces the analytical formulations for the worst-case response time, arrival-service curves, and maximum queue length. Section V describes the analytical results. In Section VI, simulations setup and achieved results are presented compared to the analytical results. Final remarks are drawn in Section VII.

II. RELATED WORKS

In IM-related literature, we can find works addressing the intersection throughput, energy efficiency, travel delays, and emission of air pollutants, among other metrics. Some of these works aim at situations with HVs only [21], [22], [23], other cases consider AVs (or CAVs) only [1], [2], [3], [4], [5], [6], while several works address traffic with mixed HVs/AVs [8], [9], [10], [11], [12], [17], which is the situation we consider in this paper.

A common aspect of many of these works is the focus on average-case metrics, be it throughput or travel delays. Worst-case metrics, such as minimum throughput, maximum travel delay, lowest energy efficiency, etc, have received much less attention. Some works already considered some worst-case aspects, though still presenting average-case results. For example, Liu et al. [25] introduced a Safe Intersection Management system for mixed HVs/AVs scenarios using a model predictive controller in which HVs follow worst-case driving behavior while AVs follow strict driving behavior.

Recently, a few works introduced worst-case performance analysis for specific IMs during specific traffic scenarios [3],

[4], [11], [12], [13], [14], [15], [16], [17]. Oza and Chantem [12] studied closely spaced intersections prone to queue spillbacks. They presented an adaptive real-time server-based approach for dynamically adjusting traffic signal timings to minimize queue spillbacks. The work also presented a worst-case analysis with bounds on wait times. As a continuation, the work in [13] complemented the time bounds on worst-case wait time and associated recovery time. Further research in [14] covered the worst-case wait time bounds for non-emergency vehicles during the presence of Emergency Rescue Vehicles (ERV). Contrarily to our work, these works do not support traffic with mixed HVs/AVs.

Miao and Leitner [16] presented traffic signal scheduling to reduce average wait time and guarantee certain worst-case wait times for CAVs. In the same line, Khayatian et al. [3], [4] propose time-aware intersection management for CAVs, only, analyzing worst-case wait times among other metrics. Contrarily, we consider mixed HV/AV traffic scenarios at complex intersections imposed by different IM approaches, not relying on CAVs.

Ghosh and Parisini [17] presented an optimization mechanism for scheduling vehicles based on their presence at a single-lane intersection. This bears similarity to our previous work in [9], [15], [26] that studied both average and worst-case vehicle delays in a mixed HV/AV traffic scenario at a single-lane intersection. However, in the current work we consider complex multi-lane intersections.

Our current work is an extension of [15] to address complex intersections and bring analytical and simulation worst-case results to a breadth of IM protocols. To the best of our knowledge, this is the only work so far specifically addressing low-speed urban settings with mixed AV/HV traffic scenarios and presenting worst-case metrics, namely the worst-case response time.

III. SYSTEM MODEL
This section describes the intersection considered in this work, states the problem, introduces the traffic models and assumptions, and analyzed IM protocols.

A. COMPLEX INTERSECTIONS
The complexity of intersections is directly related to the number of inflow lanes and crossing conflicts. In this paper, we study intersections of moderate complexity with four signalized perpendicular roadways, each with two inflow and two outflow lanes [27]. Three feasible configurations are possible depending on how the lanes are assigned to traffic crossing directions. Figure 1 shows one of those configurations, namely the dedicated left-crossing (L) and shared straight/right (S/R) crossing lanes, which is the one we consider in this paper for its popularity [27]. Figure 1 also shows the potential vehicle-to-vehicle conflicts that arise at such intersections, considering crossing, diverging, and merging conflicts. Crossing conflicts occur when vehicles from different inflow lanes going to different outflow lanes cross their paths. Diverging conflicts occur when traffic
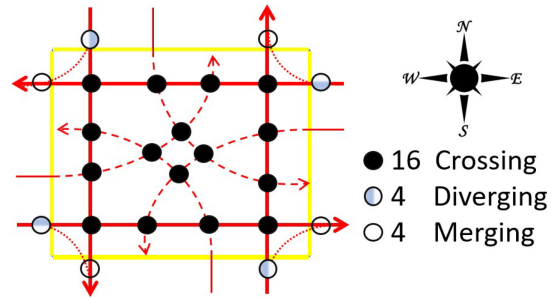

FIGURE 1. Dedicated left crossing and shared straight/right crossing lanes of a dedicated four-way two-lane intersection with potential conflicts.

from the same inflow lane splits into multiple directions. Merging conflicts occur when traffic from different inflow lanes merges into the same outflow lane.

B. PROBLEM STATEMENT
Consider a signalized intersection, as shown in Fig. 2, managed by a traffic lights control (TLC) unit that permits vehicles from all inflow lanes according to a given IM protocol. Each road leading to the intersection has at least a length L[1] that separates it from neighboring intersections. The traffic on all inflow lanes is stochastic and follows a known distribution. The problem we tackle in this work is to derive an upper-bound to the vehicles arrival curve with a sufficiently high probability that leads to worst-case service to vehicles crossing the intersection. Then, we aim to derive analytical expressions for maximum waiting time, queue size of inflow lanes and the so-called Worst-Case Response Time for different IM protocols. In particular the WCRT represents the maximum time that a vehicle may incur since it enters a road leading to the intersection until it exits the intersection and it depends on the IM and the stochastic properties of the traffic situation.

C. TRAFFIC MODEL AND SCENARIO DESCRIPTION
Figure 2 illustrates the isolated four-way two-lane road intersection with dedicated left lanes that we consider in this work. Lanes are referred to as R_{ij} where i is the road index, and j is the lane index in each road. For convenience, the road index is separated for inflow lanes ($i = 1, 3, 5, 7$) and outflow lanes ($i = 2, 4, 6, 8$). The lane index is 1 for the outermost lane and 2 for the innermost lane. The index m indicates the crossing directions of vehicles, i.e., $m = 1$ for right-crossing, $m = 2$ for straight-crossing, and $m = 3$ for left-crossing. Each road is associated with roadside units (RSU) for providing communication between AVs and road infrastructure like the IM decision-making unit. The roadside sensors $P1$ (complex induction loop detectors and cameras) and $P2$ (simple induction loop detectors) are placed on roads to detect vehicles presence. The operation of IM protocols for road lanes i and j is indexed as IM_{ij}. As referred before,

---

[1]Without the risk of confusion, we use L to refer to the left-crossing lane and L to refer to the lane length.
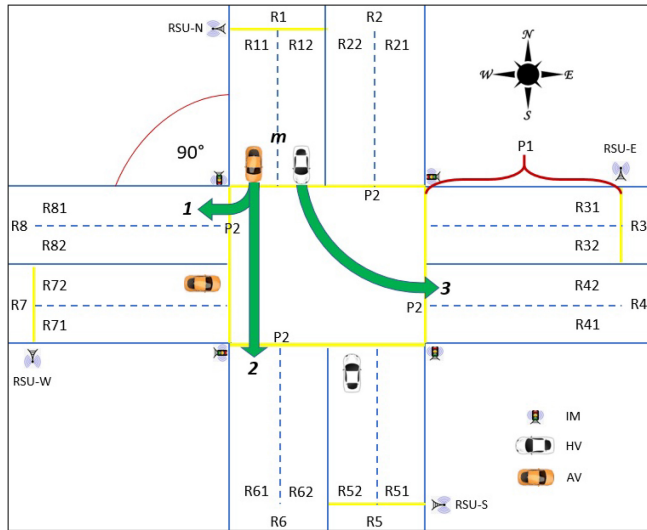
**FIGURE 2.** Complex signalized intersection with dedicated left lanes, with an orthogonal arrangement.

(a) Round-Robin. (b) MCA, TTLC, ITLC, and QTLC.

FIGURE 3. Control phases of intersection management protocols used for comparison.

each road has a length L and can hold input queues up to that size. The queue that may develop in inflow lane R_{ij} is referred to as Q_{ij}. For convenience and without loss of generality, we consider all vehicles of the same length l. We also consider a safety distance d_s between consecutive vehicles (or inter-vehicle distance) to mitigate potential rear-end collisions.

With these assumptions, we can define the capacity C of any inflow lane R_{ij} as the maximum number of vehicles that fit in the respective road length L, thus $C(R_{ij}) = \frac{L}{l+d_s}$. Here, capacity C is a constant for all inflow lanes but could vary in asymmetrical intersections. As an illustration, given a road length of $L = 400m$, vehicles with length $l = 5m$ and a safety distance of $d_s = 5m$ lead to a capacity of $C = 40veh$ for all inflow lanes. In any inflow lane, the maximum queue size Q_{max} should never exceed the capacity C to prevent queue spillback from occurring [12].

We also observe that all IM protocols exhibit what we call a *control cycle*, referred to as Φ_{IM}. This cycle arises from the pattern of serving inflow lanes and is formed by a set of phases that repeat indefinitely, including green and yellow phases, as appropriate.[2] The total time required to execute one complete intersection control cycle Φ_{IM} is $T_{\Phi_{IM}}$. In each control cycle, the maximum number of vehicles that each IM protocol will be able to discharge (serve) from an arbitrary inflow lane R_{ij} is $D_{IM_{ij}}$.

Suppose $\lambda_{ij}(t)$ in veh/s is the instantaneous traffic arrival rate at time t on lane j of road i. At the beginning of the kth control cycle that starts at time t, a certain number of vehicles are queued in the respective queue $Q_{ij}(k)$ waiting to access the intersection. The state of the queue in the inflow road i lane j at the beginning of the following control cycle ($(k +$
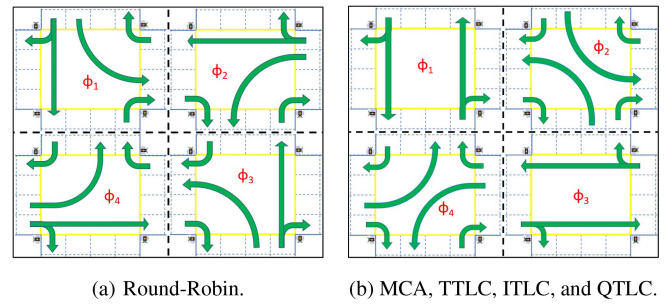
$1)^{th}$) is a function of the queue size in the previous cycle, the arrival rate integrated into the current cycle, the IM policy and the lane capacity, $Q_{ij}(k + 1) = f(Q_{ij}(k), \lambda(t), IM, C)$.

Finally, we assume that lane changes near the intersection are prohibited and that vehicles respect the "first-in-first-out" (FIFO) rule without U-turns. We also consider the intersection features a TLC, sensors and roadside units (RSUs) that each IIM needs to operate properly.

D. COMPARING INTERSECTION MANAGEMENT PROTOCOLS

The remaining part of this section briefly presents the six IM protocols employed in this paper, namely RR, TTLC, MCA, ITLC, QTLC, and SIMP, to compare the WCRT of vehicles that these IM approaches provide.

Round-Robin (RR) IM strategy was developed based on the RR scheduling algorithm of Operating Systems. RR is a conventional pre-configured IM strategy that rotates green-yellow phases in a circular order for a fixed allocated time. The RR IM strategy serves vehicles from one roadway at a time in a fixed direction [28]. The RR IM approach is also called the uniform TLC due to the uniformly distributed green and yellow phases. We consider the RR IM approach with the typical improvement that enables right-crossing vehicles from all non-conflicting road lanes. The RR IM control phases are shown in Fig. 3(a) for a four-way two-lane dedicated left-crossing intersection. We consider the RR configuration suggested in [26] with each green phase taking 30s and being followed by a 4s yellow phase.

Trivial Traffic Light Control (TTLC) strategy is another conventional pre-configured IM strategy operating for a fixed time. Unlike the RR IM strategy, TTLC serves vehicles from two opposite directions simultaneously alternating between North-South and East-West [20]. The control phases for a four-way two-lane dedicated left-crossing intersection are illustrated in Fig. 3(b). TTLC permits the vehicles of straight/right-crossing lanes for this particular intersection type first (ϕ_1) and then switches to the left-crossing lanes (ϕ_2). The original configuration used by [20] gives control to the driver instead of the IM on the left-crossing lanes while permitting the opposite shared right lanes. We adapted the original configuration by separating the left and shared right lanes. In this configuration, the shared right lane gets

---

[2]We do not refer to red phases since these always correspond to green or yellow phases in another inflow lanes, which are the phases during which vehicles are actually served.

a green time of 30s (S/R), and the dedicated left lane gets 15s (L), both followed by a 4s yellow phase.

Max-pressure Control Algorithm (MCA) was initially employed in communication networks for message scheduling. The same idea has been applied in managing signalized [21], [22] and autonomous [6] intersections. MCA optimizes TLC signals by measuring adjacent lanes traffic flow (number of vehicles) and assigning weights to turn movements. Therefore, MCA improves the intersection throughput by stabilizing the queue pressure acyclically. We have tested several control configurations as in Fig. 3 and minimum green times (5s, 15s, and 30s) and found that the control phases shown in Fig. 3(b) with 30s of green time followed by 4s yellow time to be the most efficient.

Intelligent Traffic Light Control (ITLC) is an IIM strategy that employs real-time traffic characteristics (queue length, vehicle speed, waiting time, and acceleration) to determine traffic light phases, their order, and execution length towards better traffic fluidity and reduced waiting time [2]. A road lane with a longer queue length and its opposite lane gets a proportionally longer green phase until a fixed maximum duration of 60s followed by a 4s yellow phase. The lanes with the shorter queue values get a minimum green phase time of 5s, thus, the ITLC control phases form a cycle. The ITLC control phases for a four-way two-lane dedicated left-crossing intersection are shown in Fig. 3(b).

Q-learning based Traffic Light Control (QTLC) is also an IIM strategy that was designed as a multi-agent system for reducing vehicle waiting time [23]. QTLC utilizes queue length, waiting time, and elapsed phase time for TLC decision-making, resulting in either continuing with the current phase or switching to the next phase. QTLC is configured with a minimum (20s) and maximum (60s) green phase duration, and then switching to another phase can only be triggered after the initial 10s and before the last 10s of the phase. Green phases (Fig. 3(b)) are interleaved with a 4s yellow phase.

Synchronous Intersection Management Protocol (SIMP) was introduced to provide traffic fluidity within the intersection and manage mixed HVs and AVs [24]. SIMP is said to be synchronous as it iterates the following steps in cycles according to the pattern shown in Fig. 3(b). On the road architecture shown in Fig. 2: finding vehicles at the intersection entrance, detecting their intended crossing directions using sensors, deciding vehicles safe crossing using a *Conflicting Directions Matrix* (CDM) and waiting for admitted vehicles to exit the intersection. The CDM lists the crossing conflicts (Fig. 1) of the intersection and allows SIMP to identify conflicting maneuver intentions when checking all inflow road lanes simultaneously at every control cycle.

IV. ANALYTICAL MODELS

As mentioned before, we are interested in analyzing the performance of IM protocols under worst-case conditions. In particular, we focus on the so-called Worst-Case Response Time (WCRT) and upper and lower bounds to traffic arrival and service curves, respectively.

A. NOTATION

To facilitate the understanding of the WCRT analysis, first, we introduce the most relevant notation used.

- R_{ij} is the road lane index in the intersection (for $i = 1, \ldots, 8$ and $j = 1, 2$);
- m is the crossing direction ($m = 1, 2, 3$ for right, straight, left);
- L is the road length to and from the intersection;
- v_s is the saturation speed s of vehicle v;
- l is the length l of vehicles;
- d_s is the minimum safe distance between consecutive vehicles;
- $C = \frac{L}{l+d_s}$ is the road capacity;
- Q_{max} is the maximum number of vehicles that queue up across all road lanes;
- $WCRT_{IM_{ij}}$ is the worst-case response time (WCRT) provided by the concerned IM protocol for road lane R_{ij};
- $WCIST_{IM_{ij}}$ is the worst-case intersection service time (WCIST) provided by the concerned IM protocol for road lane R_{ij};
- QT_{ij} is the vehicle queue joining time on road lane R_{ij};
- $WT_{IM_{ij}}$ is the vehicle waiting time imposed by the IM on road lane R_{ij};
- ICT_m is the intersection crossing time of crossing direction m;
- $\Phi(IM)$ is the set of phases that compose the intersection control cycle under a given IM protocol, including green $\phi_g = (\phi_1, \phi_2, \phi_3, \phi_4)$ and yellow (ϕ_y), as appropriate;
- $T_\Phi(IM)$ is the time required for the execution of one complete intersection control cycle $\Phi(IM)$;
- $\mathcal{D}_{IM_{ij}}$ is the number of vehicles that the IM approach serves per road lane R_{ij} during the green phase;
- $n = \lceil \frac{Q_{max}}{\mathcal{D}_{IM_{ij}}} \rceil$ is the number of control cycles that Q_{max} vehicles must wait before being served;
- $\alpha(t)$ is the cumulative arrival function of vehicles at an intersection;
- $\mu(t)$ is the cumulative service function of vehicles dispatched from an intersection;
- λ is the long-term average arrival rate;
- s is the saturation flow rate;
- x is the number of vehicles in a queue under analysis;
- x_s is the number of queued vehicles needed to trigger saturation;

B. WORST-CASE RESPONSE TIME

We define the WCRT in an intersection as the time that mediates between the moment a vehicle enters the road leading to the intersection and the moment that vehicle leaves the intersection. In the absence of a queue, the WCRT can be the traveling time at an average speed that the

vehicle travels. However, the queuing due to concurrency in the access to the intersection causes extra delay. The time that mediates between a vehicle arriving at the queue and leaving the intersection is called the intersection service time (IST). In other words, the IST is a combination of waiting time (WT) and intersection crossing time (ICT). Worst-case concurrency will lead to the worst-case intersection service time (WCIST).

Both WCRT and WCIST are specific per IM protocol and per lane, thus, we refer to them as $WCRT_{IM_{ij}}$ and the corresponding $WCIST_{IM_{ij}}$. In our case, and without loss of generality, we consider the four roads symmetrical; thus, we have just two different cases, those of the left and the right lanes in any road.

Suppose that we can determine Q_{max}, i.e., the maximum number of vehicles that queue up across all road lanes. Then we can estimate the $WCRT_{IM_{ij}}$ as in Eq. (1), by adding the time the vehicle takes from the beginning of the road to the queue tail (i.e., QT) using the length of the maximum queue Q_{max} (considering that it travels at speed v_s) with the respective $WCIST_{IM_{ij}}$.

$$WCRT_{IM_{ij}} = \frac{L - Q_{max} \times (d_s + l)}{v_s} + WCIST_{IM_{ij}} \quad (1)$$

We can use Eq. (2) to estimate $WCIST_{IM_{ij}}$ knowing the WT and ICT.

$$WCIST_{IM_{ij}} = WT_{IM_{ij}} + ICT_m \quad (2)$$

The WT that the IM system imposes on vehicles per road lane R_{ij} can be estimated using Eq. (3) shown at the bottom of the page, an adapted version of Eq. (2) presented in [29]. When the Q_{max} is less than $D_{IM_{ij}}$ during a green phase (ϕ_g), two situations can happen. Either an arriving vehicle crosses the intersection in that phase and its $WT = 0$ (we refer to this condition as ϕ_g) or, if the phase ends before that vehicle crosses, it will have to wait for the next green phase in the following cycle, thus $WT = T_{\Phi_{IM}} - \phi_g$. If, under sufficiently dense traffic, the Q_{max} grows beyond $D_{IM_{ij}}$ in a single TLC cycle, then a vehicle may have to wait stopped for $n-1$ full TLC cycles plus the maximum time to the next green phase, where n is the number of TLC cycles needed to serve the Q_{max} vehicles. These three cases are expressed in Equation (3).

The second component of the WCIST is the ICT (s/veh), which is the time required to traverse the intersection. The ICT is measured between the entrance and exit of the intersection and is different for different crossing directions, i.e., $m = 1, 2, 3$. For the sake of simplification, we consider two different crossing times: to turn right (shorter for $m = 1$) and to cross straight or turn left (longer for $m = 2, 3$).

Finally, to determine Q_{max}, we need to analyze the balance between traffic arrival patterns and the intersection service.

C. SATURATION SPEED

Saturation occurs when the road lanes are congested due to queue buildup induced by the downstream bottleneck (i.e., the signalized intersection) and associated IM operations affecting the upstream traffic [30]. During saturation traffic conditions, vehicles do not travel at the free-flow speed but at a lower speed instead, called saturation speed. This is the speed (v_s) used in Eq. (1) to compute $WCRT$ values. The saturation speed depends on the geometric settings of the intersection, flow density and traffic conditions, road lane width, traffic signal timing, IM operations, and vehicle properties, e.g., whether HVs or AVs. This has been extensively studied by [31]. Conversely, this paper determines the saturation speed with actual values acquired from the SUMO simulator. Computing the saturation speed as done by [31] is left for future work.

D. ARRIVAL AND SERVICE CURVES PER INFLOW LANE

Flow analysis and queuing theory have long been used to compute queue length and service time estimates in traffic scenarios [32]. Considering an intersection with a given IM protocol, a cumulative service function tells us how many vehicles the intersection can serve from a given lane up to time t. Moreover, a cumulative traffic arrival function per inflow lane provides the number of vehicles arriving at the intersection in that lane up to time t. The difference between the arrival and the service curves at time t gives us the number of vehicles queued at the intersection in that lane, waiting to be served. Similarly, the *IST* for a given number of vehicles can be computed by the difference between the time they arrive together at the queue and the time the last one is served.

The cumulative service function, typically designated $\mu(t)$, is frequently easy to derive, knowing the control cycle of the specific IM protocol and its configuration parameters. On the other hand, the traffic arrival is normally stochastic and thus impossible to define precisely. However, it is frequently possible to upper bound it, even if with a residual probability of exceedance, if it follows a known distribution. A common upper bound, typically designed $\alpha(t)$, is shown in Eq. (4).

$$\alpha(t) = \begin{cases} s \cdot t & \text{if } t < x_s/s \\ x_s + \lambda \cdot t & \text{otherwise} \end{cases} \quad (4)$$

An initial burst[3] reaches x_s number of vehicles, sufficient to trigger saturation (hence being called saturation flow

[3]Rarely unexpected injection of vehicle traffic in large volumes.

$$WT_{IM_{ij}} = \begin{cases} 0, & \text{if } Q_{max} \leq D_{IM_{ij}} \& \phi_g \\ T_{\Phi_{IM}} - \phi_g, & \text{if } Q_{max} \leq D_{IM_{ij}}; \\ (n-1) \times T_{\Phi_{IM}} + (T_{\Phi_{IM}} - \phi_g), & \text{if } D_{IM_{ij}} < Q_{max} \leq nD_{IM_{ij}}. \end{cases} \quad (3)$$

volume) and arrives at the saturation flow rate[4] s. Then, the following vehicles arrive equally spaced at a long-term average rate λ.

Therefore, knowing the arrival upper bound and the service functions allows deducing an upper bound to the queue length as in Eq. (5), subject to $\alpha(t) > \mu(t)$, and to the *WCIST* as in Eq. (6), subject to $\mu^{-1}(x) > \alpha^{-1}(x)$.

$$Q_{max} = \max_t(\alpha(t) - \mu(t)) \qquad (5)$$

$$WCIST = \max_x\left(\mu^{-1}(x) - \alpha^{-1}(x)\right) \qquad (6)$$

Note that Eq. (6) allows computing WCIST with any service curve μ, while Eq. (2) already assumes a specific IM service policy. On the other hand, the value of Q_{max} provided by Eq. (5) allows solving Eqs. (2) and (1) to deduce *WCIST* and *WCRT* values, respectively.

Finally, for the stability of the intersection system, it is necessary that the long-term average arrival rate λ is always lower than the average service rate $\bar{\mu}$.

V. WORST-CASE IM PERFORMANCE ANALYSIS

This section analyzes the analytical models presented earlier. We use the long-term traffic arrival rates and IM-specific service rates to draw the arrival-service curves, and then find out Q_{max} and *WCIST* values. These are examined per road lane per IM approach.

A. VEHICLE ARRIVAL PATTERNS

Our concrete case considers all roads leading to the intersection to have a length of $550m$. This road length is divided into the intersection area with $L = 500m$ and the traffic injection area with $50m$. Figure 2 illustrates the intersection area with two inflow/outflow lanes where the queue length Q can be measured. The traffic injection area is a single-lane road that initiates and distributes the arriving traffic to the two inflow lanes according to the target directions. We consider an equal distribution for the three directions, i.e., 33%. The aforementioned settings are identical to the ones employed in [24]. Therefore, we utilize the throughput results of [24] to select the saturation flow rate, in which different IM systems saturate at different rates between $0.2veh/s$ and $0.4veh/s$. Here we use $0.4veh/s$ as the saturation flow rate to enforce saturation for all IM systems. This rate is distributed among the two inflow lanes according to the traffic volume per direction and the directions served per lane. For the dedicated left lane $s = 0.133veh/s$ (33% left-crossing vehicles) and for the straight and right-crossing lane $s = 0.266veh/s$ (33% of straight-crossing plus 33% of right-crossing vehicles).

These flow rates are used to draw the arrival curves using Eq. (4). Since we do not know the saturation flow volume x_s, we consider just the saturation flow rate and not the long-term rate that is lower, thus upper bounding vehicles arrival. It is also important to recall the capacity of $500m$

TABLE 1. IM specific cycle and green times, and the corresponding number of vehicles that can be served at different maximum speed settings.

IM	Cycle Time (s)	Green time (s) (Lanes S/R and L)		No. of vehicles			
				30km/h		50km/h	
		S/R	L	S/R	L	S/R	L
SIMP	11	2.5	3	3	1	3	1
RR / MCA	136	30	30	12	12	14	14
TTLC	106	30	15	12	6	14	7
ITLC / QTLC	166	60	15	24	6	28	7

long lanes, with $5m$ long vehicles and $5m$ safety distance, i.e., the maximum number of vehicles that can be queued in any one lane is $C = 50veh$.

B. VEHICLE SERVICE PATTERNS

The service that the intersection can provide in terms of crossing vehicles depends on the IM protocol used and the maximum speed allowed. The maximum speed makes a stronger impact in protocols with longer green times since more vehicles cross per green phase. On the other hand, for worst-case conditions, we consider that no vehicles are served in the yellow phases. These are used just to flush vehicles admitted at the end of the preceding green phases.

Therefore, based on the properties of the IM protocols described in Section III and the two maximum speeds considered in urban environments ($30km/h$ and $50km/h$), we present in Table 1 the number of vehicles that each IM serves from each lane per cycle. The referred maximum speeds are suggested by the European Commission for Road Safety in urban environments, namely $30km/h$ for urban residential areas and $50km/h$ for urban non-residential areas.[5]

Note that SIMP permits per cycle (Fig. 3(b)) at least one vehicle per L lane and three vehicles per S/R lane. On the other hand, ITLC and QTLC adapt their green time based on the instantaneous queue length, waiting time, the distance from the intersection entrance, and their accelerations. In this case, we consider the maximum green time of $60s$, which would correspond to having no cars arriving on the other roads and lead to longer cycle time.

C. ARRIVAL-SERVICE CURVES

To draw the specific arrival and service curves that apply to our case, we consider that the system is empty at $t = 0$; thus, $Q(0) = 0$, and only then accumulates vehicles. Also, note that this is a worst-case traffic scenario. Thus each IM approach starts (at $t = 0$) at the beginning of the phase that immediately succeeds the phase of the respective lane, thus waiting for a control cycle to start serving vehicles.

Figure 4 shows the arrival curve $\alpha(t)$ and service curves $\mu(t)$ for the different IM protocols, for both maximum speeds employed, i.e., $30km/h$ and $50km/h$. The vertical axis represents the cumulative number of vehicles that arrive/leave the intersection. Figure 4 also shows the case
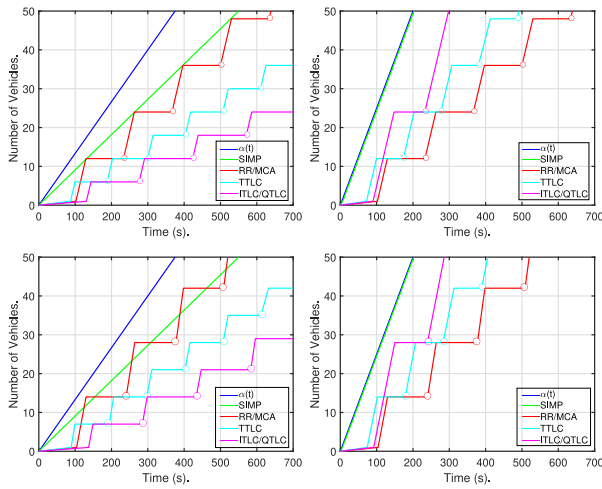
FIGURE 4. Arrival and service curves at 30km/h (top) and 50km/h (bottom), for the dedicated left lane (left) with $s = 0.133\,veh/s$, and a shared right lane (right) with $s = 0.266\,veh/s$.

of the dedicated left lane intersection with $s = 0.133\,veh/s$ (left plots) and $s = 0.266\,veh/s$ (right plots).

We also represent the arrival and SIMP service curves as linear, given the increments of just one vehicle at a time. Conversely, all other service curves have a clear step-wise pattern with the step size given by the number of vehicles each IM processes per control cycle (Table 1).

Among all IM protocols, SIMP shows the highest average service rate. However, the case of SIMP shared right lane (S/R) requires clarification since the service rate of the right lane ($3\,veh/11s = 0.27\,veh/s$) would be higher than the arrival rate ($0.266\,veh/s$), thus violating the $\alpha(t) > \mu(t)$ condition needed to have traffic accumulation. In this case, we consider that the service rate is truncated to the arrival rate (naturally, the intersection cannot serve more vehicles than those arriving). All other IM protocols respect this condition, thus leading to traffic accumulation.

Another important observation is the relative performance in the average service rate of the other IM protocols beyond SIMP. While RR and MCA serve equally (12veh per cycle, for the left and right lanes, respectively), the left and right lanes (red traces), TTLC, ITLC, and QTLC show a significant asymmetry, which is more pronounced for ITLC and QTLC (6veh against 24veh per cycle) than for TTLC (6veh against 12veh per cycle). These differences invert the order of the average service rates of these protocols. On the left lane, both TTLC, ITLC, and QTLC are worse than RR/MCA, with ITLC and QTLC being the worst given their relatively poor service in the left lane. Conversely, in the right lane, both TTLC, ITLC, and QTLC are better than RR/MCA, with ITLC and QTLC being the best given their relatively better service.

Figure 5 shows a more expressive version of the dedicated left lane at 30km/h maximum speed (upper left plot) of Fig. 4 in which we consider an arriving burst of 50veh injected. We then extended all service curves until they reach 50veh

so that we can compute for all cases the *WCIST* and Q_{max} according to Eqs. (5) and (6).

With SIMP, the last vehicle in each cycle suffers a longer waiting time, given the protocol serving just one vehicle per cycle per lane. Unlike SIMP, in all other IM approaches (RR, MCA, TTLC, ITLC, and QTLC), the first vehicle in each cycle suffers the longest waiting time compared to the other vehicles served in the same cycle (each step). The small circles in the service curves indicate the vehicles that suffer the worst service (Figs. 4 and 5), and it can be confirmed by visually inspecting the vehicles marked to have a larger time interval (x-axis distance) to the arrival curve (blue line) than those at the end of a cycle. The reason is that the first vehicle, in the worst-case, arrives at the intersection entrance when the current red phase starts, thus having to wait for the green phase of the next cycle. Conversely, a vehicle arriving during the red phase when other vehicles are already queued will have to wait for less time for the beginning of the following green phase. Then, during the green phases, the waiting time is also reduced since the dispatch rate is at the maximum speed (see the inclination of the service curves when transitioning between steps). Since the dispatch rate is higher than the arrival saturation rate, traffic accumulation reduces during the green phases.

The maximum vehicle queue length Q_{max} shows how congested the road lane is and specifies the efficiency of IM protocols in tackling the saturation flows. Due to its short control cycle length, SIMP is again the best IM in this aspect, with the lowest Q_{max} values for all cases in the various tested arrival rates. The other IM approaches show different Q_{max} behaviors depending on their control cycle time.

Finally, we have also studied the arrival-service curves, Q_{max}, and *WCIST* of all IM protocols at an increased maximum speed of 50km/h (lower plots of Fig. 4). The achieved results are similar for SIMP since it continues serving the same number of vehicles per cycle. For all other IM protocols, the service is increased since more vehicles can cross the intersection per phase of the control cycle (Table 1). Consequently, we observe a reduction in the respective values of Q_{max} and *WCIST*.

D. DETERMINING MAXIMUM QUEUE LENGTH AND INTERSECTION SERVICE TIME
One possible way of finding Q_{max} directly consists of direct measurements with the help of deployed road infrastructure. Alternatively, if the distribution of the traffic arrival pattern is known, then it is possible to compute the maximum arrival of vehicles in a given interval with a certain probability. We call them sensor-based and stochastic-based approaches.

1) SENSOR-BASED MAXIMUM QUEUE LENGTH DETERMINATION

In this approach, the queue length is measured using deployed sensors, such as induction loop detectors and
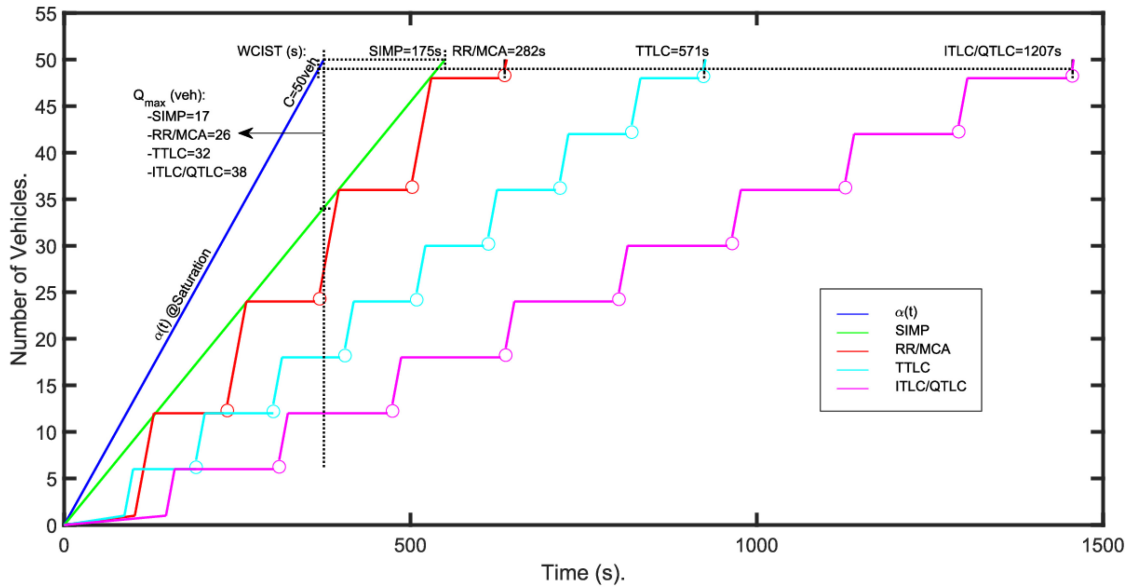
FIGURE 5. Blue: upper bound of the arrival curve at saturation flow conditions; other colors: lower bound of service curves of IM approaches. Dashed horizontal lines show the estimated WCIST with an injected burst of 50veh. Dashed vertical lines shows the estimated Q_{max} for each IM with the same injected burst for each IM.
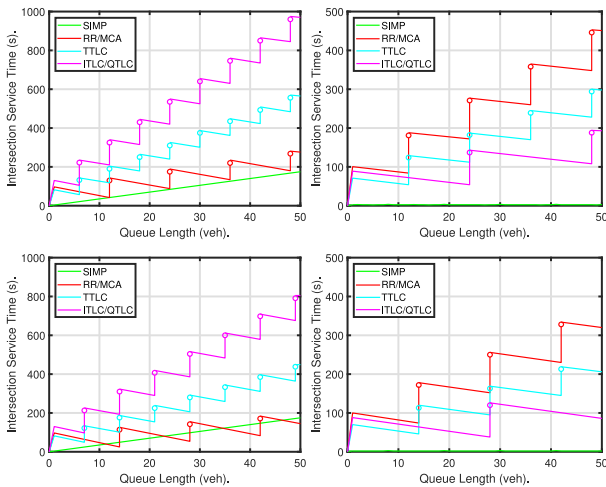
FIGURE 6. Intersection service time (IST) in seconds as a function of the queue length in *veh* for 30*km/h* (top) and 50*km/h* (bottom) maximum speeds and for the dedicated left lane (left) and shared right lane (right).

cameras, as well as vehicle-to-infrastructure (V2I) communications if available. Then, Q_{max} is estimated after observing the queue length for a sufficiently long interval. Knowing Q_{max}, WCIST can be obtained directly from Eq. (2).

Figure 6 displays the IST for the last vehicle in the queue as a function of the queue length for all IM protocols and both dedicated left and shared right lanes (corresponding to the same cases in Figure 4). The results indicate that the vehicles in the left lane (left plots) suffer longer waiting times for all IM approaches than vehicles in the right lane (right plots), except RR and MCA. This is due to the lower bandwidth of the service provided by the IM protocols in the left lane, except for the two referred. Remember that SIMP, in the right lanes (right plots), can serve the saturation

arrival rate without queuing, thus the *ICT* is constant and the lowest possible, at 5s.

Finally, Figure 6 also shows the effect that *IST* reduces during service phases, as we discussed already. The *WCIST* per service phase occurs for the first vehicle of that phase (queue sizes immediately after the small open circles).

2) STOCHASTIC-BASED BURST DETERMINATION

In this case, we consider that the traffic arrival pattern follows a known distribution. In this paper, we consider a Poisson distribution (Eq. (7)) since the vehicles arrive independently of each other. Knowing the distribution, we can compute the maximum number of vehicles (x) arriving in a specific interval t given the desired probability. We use this to determine the saturation volume x_s with two desired probabilities (or confidence levels), namely 99% and 99.9%. Then we can deduce Q_{max} using Eq. (5).

$$P(x \text{ vehicles in interval } t) = \frac{(\lambda t)^x e^{-\lambda t}}{x!} \qquad (7)$$

One interesting feature of this approach is that, for each desired probability, Q_{max} comes as a function of the long-term average vehicles arrival rate λ, with Q_{max} bounded by the lane capacity C and λ constrained to be less than the corresponding saturation flow rate s. Thus, knowing λ we can compute x_s and Q_{max}. To compute x_s, we increment the number of vehicles x one by one, computing for each number the time t corresponding to the arrival of x vehicles at the saturation flow rate s. We use these values in Eq. (7) and compute the associated probability. We increment x until the achieved probability exceeds the defined threshold (confidence level).

The left plot of Figure 7 presents the values of x_s using Eq. (7) with probability values of 99% and 99.9%.

(a) x_s and burst (veh).

(b) WCIST for the left lane (L).

(c) WCIST for the right lane (S/R).
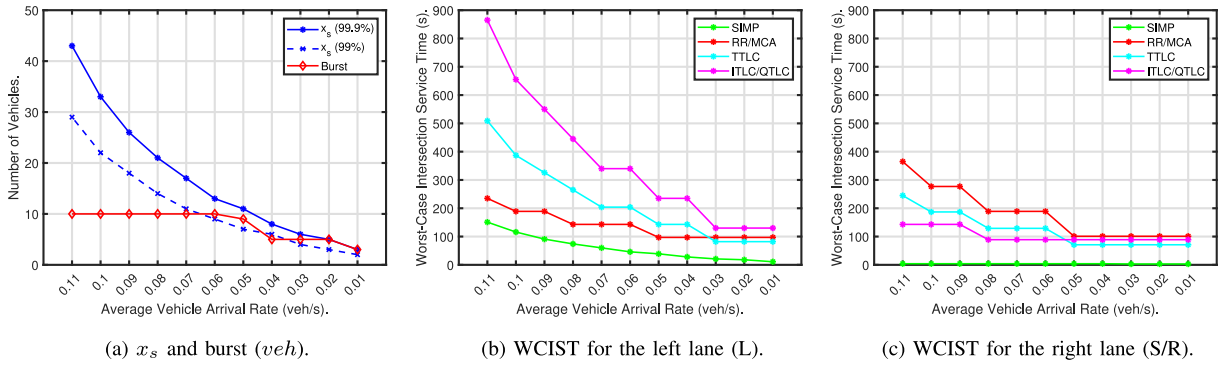
FIGURE 7. Maximum burst x_s (left) and *WCIST* against the long-term average vehicle arrival rate in veh/s considering x_s values with 99.9% confidence for left lanes (center) and right lanes (right).

It also shows the observed maximum vehicle burst (via SUMO simulator) as a function of λ (left plot). We used a single inflow lane with a single injecting point to obtain these values with inter-injection times below $4s$. Note that these values, i.e., vehicle arrivals, are independent of the intersection. The maximum burst was observed in SUMO during a simulated time of 40h and using the vehicle parameters in Table 2. We observed a burst behavior that grows for growing values of λ until $0.06veh/s$ and then saturates at $10veh$. We believe SUMO induces this saturation, but the concrete reason remains to be uncovered. More interestingly, the observed bursts for lower values of λ are between the value of x_s for the probabilities of 99% and 99.9%.

Figure 7 also presents the *WCIST* values provided by the different IM approaches using Eq. (6) (center plot for the left lane and right plot for the right lane) and associated with x_s values of 99.9% confidence. Though not shown, the WCIST values for x_s values with 99% confidence are necessarily lower or equal, given that fewer cars arrive with this probability. For these WCIST values, first, we calculate the IST values for each vehicle on each road lane, which will serve as the WCIST based on the Q_{max} estimated earlier for each road lane. Thus the maximum value of the WCIST of all inflow lanes can be considered as the WCIST of the entire IM approach with respect to λ.

VI. SIMULATION-BASED CHARACTERIZATION
This section is divided into six subsections. First, we introduce the simulation settings employed throughout this paper, followed by the observed Q_{max} values respecting the comparing IM approaches for various long-term average arrival rates (λ). Then the lane throughput results are presented. The response time of non-saturated and saturated traffic flows is presented before validating the analytical WCRT values with the observed WCRT results.

A. SIMULATION SETUP
To validate the analytical results, we ran simulations using the urban mobility simulator (SUMO) (v1.13.0) [18]. As of our analytical analysis, the six IM protocols (SIMP,

TABLE 2. Simulation parameters and assigned values.

Parameters	Values
Road Network Area	$1020 \times 1020\ m^2$
Vehicle Type	HVs (Krauss) and AVs (ACC)
Vehicle Length	5 meters
AVs rate	50%
Safety distance (target)	5 meters
Max. Speed	$30km/h$ and $50km/h$
Acceleration	$2.6m/s^2$
Deceleration	$-4.5m/s^2$
Emergency Deceleration	$-9m/s^2$
Minimum Time Headway	$1s$
HV Drivers Imperfection	0.5

RR, MCA, TTLC, ITLC, and QTLC) were applied to an isolated four-way two-lane intersection with dedicated left lanes. Two maximum speeds ($30km/h$ and $50km/h$) were tested with acceleration ($2.6m/s^2$), deceleration ($-4.5m/s^2$), and emergency deceleration ($-9m/s^2$) respecting typical urban mobility settings. We have employed the SUMO default values for HVs (Krauss [33]) and AVs (adaptive cruise control - ACC [34]) representing car-following model-specific parameters, such as the minimum time headway (the time/space distance between a car front bumper to the preceding car back bumper), set at $1s$, and the driver imperfection parameter, set at 0.5. The summary of simulation parameters and assigned values are listed in Table 2. These are the default values suggested for passenger cars by the SUMO simulator representing common values observed in practice.[6]

For Q_{max} (Fig. 8) and throughput (Fig. 9), the traffic generation follows the Poisson distribution similar to what we considered in the previous section. However, we separated the injection into the two lanes of each road instead of using a single injection as we described before. This separation was relevant, here, to fully respect the generation distribution per lane, avoiding the potential interference that the single injection point could create.

[6]https://sumo.dlr.de/docs/Vehicle_Type_Parameter_Defaults.html
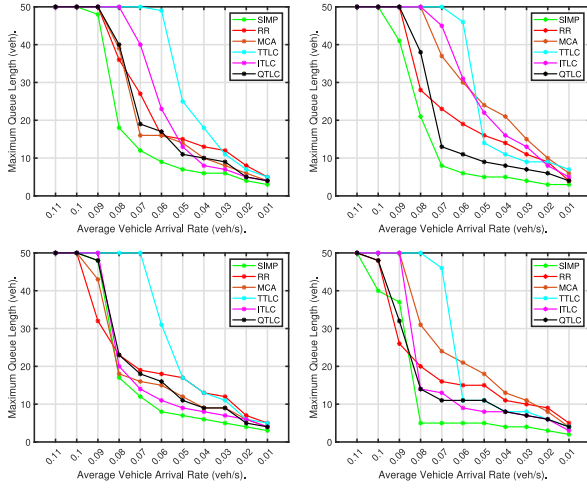
FIGURE 8. IM induced Q_{max} in *veh* against the long-term average vehicle arrival rate in *veh/s* for the left-crossing lane (left) and right lane (right) at $30km/h$ (top) and $50km/h$ (bottom) maximum speeds and capacity $C = 50veh$.

FIGURE 9. Lane throughput in *veh/s* against the long-term average vehicle arrival rate in *veh/s* for L-crossing (left) and S/R-crossing (right) lanes at $30km/h$ (top) and $50km/h$ (bottom) maximum speeds and capacity $C = 50veh$.

Using two-lane intersections (Fig. 2) with $20m$ width, the observed ICT values are under $\sim 1s$ (R-crossing) and $3s$ (L/S-crossing) for both AVs and HVs at $30km/h$. When the vehicles are stopped and waiting to access the intersection, it takes approximately $2s$ for the first vehicle to react to the green signal. The following vehicles add up a gradually smaller reaction time, which is called the start-up lost time [35]. Altogether, we consider $ICT_1 \leq 3s$ (R-crossing) and $ICT_{2,3} \leq 5s$ (S- and L-crossing). For convenience, we later do a pessimistic assumption and consider $ICT_m \leq 5s, \forall_m$ to estimate the WCIST value at all speeds.

Finally, the implementation of all six IMs in SUMO was validated independently in the simulations using the vehicle FCD data and confronting it with the phases and rules of each IM.

B. MAXIMUM QUEUE LENGTH

For Q_{max} analysis, we analyzed traces of $30h$ of simulated time with various long-term average arrival rates, namely $\lambda = 0.01$ to $0.11veh/s$. We measure Q_{max} by counting the vehicles from the intersection entrance until the last consecutive vehicle moving at or below $5km/h$. Figure 8 illustrates the observed Q_{max} for both maximum speeds, i.e., $30km/h$ (top) and $50km/h$ (bottom) for both the left lane (left) and the right lane (right).

At $30km/h$ maximum speed, SIMP shows the best performance on both lanes with lower Q_{max} values. Particularly, SIMP-produced Q_{max} is below $10veh$ with up to $0.06veh/s$ in the left lane and up to $0.07veh/s$ in the right lane. For the same arrival rates, the Q_{max} of TTLC reaches the lane capacity being the worst performing approach. The other IM approaches show, in the left lane, a closely interchangeable relation among RR, MCA, ITLC, and QTLC where ITLC reaches the lane capacity level first. In the right lane, QTLC is the second best-performing approach after SIMP for lower arrival rates. In general, most IM
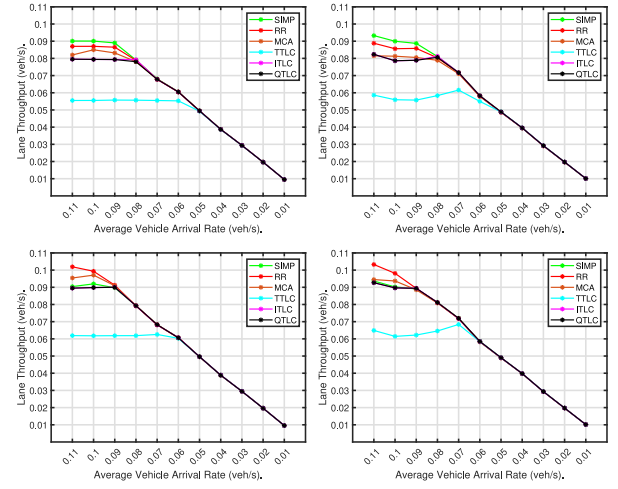
approaches start saturating for λ above $0.05veh/s$. After TTLC, the order IM approaches to reach the lane capacity are ITLC and MCA, QTLC and RR, and in the end, SIMP. Similar observations can be made with the maximum speed of $50km/h$.

SUMO also provides a direct assessment of Q_{max} in each of the simulation traces. In most cases, both SUMO and our sensor-based approaches provide similar results with a difference of one to two vehicles. In a few cases, the SUMO-produced Q_{max} results are much higher. A possible reason is that SUMO may consider vehicles moving below $5km/h$ speed on the entire road lane instead of consecutive from the intersection entrance.

C. LANE THROUGHPUT

The lane throughput can be defined as the number of vehicles that completed their journeys by crossing the intersection either straight or right (S/R-crossing lane) or left (L-crossing lane) from their injection point in one hour. We used the same $30h$ long-run FCD data employed in estimating the Q_{max} to observe the achieved lane throughput. Figure 9 shows the throughput of both lanes (S/R-crossing and L-crossing) at both maximum speeds (30 and $50km/h$).

The $30km/h$ throughput results show a similar behavior among all IM approaches until $0.05veh/s$ for both S/R-crossing and L-crossing lanes, with just a small difference of $1-3veh$ among IM approaches. The performance of TTLC starts decreasing with increasing arrival rates and saturates at $0.06veh/s$, the poorest IM approach in serving dense traffic. The next saturating approaches are ITLC and QTLC at $\sim 0.08veh/s$ followed by the RR conventional IM approach achieving between $0.08veh/s$ and $0.09veh/s$. SIMP shows the highest lane throughput with at least $0.09veh/s$.

Similar throughput behaviors can be observed at the increased maximum speed of $50km/h$ for lower arrival rates until $0.06veh/s$. After this point, all IM approaches increase

their saturation throughput, because of the higher vehicle dispatch rate within their green phases. The only exception is SIMP which does not take advantage of the increase in maximum speed, thus losing its relative leading position.

D. RESPONSE TIME OF NON-SATURATED TRAFFIC FLOW

As defined earlier, the RT includes both the vehicle time to join the queue and the IST upon joining the queue. Note that the IST comprises both the queuing time and intersection crossing time. In this section, first, we present the queue joining time, then the IST, and in the end, the RT (queue joining time + IST). For this non-saturated scenario, we use the same traffic generation as in the analytical characterization, with a single injection point per road, following a Poisson distribution. The crossing directions are uniformly distributed for left (33%), straight (33%), and right (33%).

Therefore, the right lane accommodates $0.067\,veh/s$ of the injected vehicles, and the left lane accommodates the remaining $0.033\,veh/s$. We generated the FCD data for these experiments using the same SUMO simulator for 1000 vehicles injected in each road at a long-term average arrival rate of $\lambda = 0.1\,veh/s$.

1) QUEUE JOINING TIME

Queue joining time is when vehicles approach the intersection entrance or join the queue before accessing the intersection. We consider that in this period they travel close to the maximum speed. However, vehicles are injected with zero speed, taking about $4s$ to reach maximum speed. This may influence the following injected vehicles to comply with the safety distance. Whenever a burst of vehicles is injected with inter-injection times below $4s$, the following vehicles speed profiles are adjusted so they respect the minimum inter-vehicle distance. This creates a leader-follower dependency following the first vehicle in the burst. This may lower the actual travel speed of the vehicles, thus influencing the queue joining time.

Figure 10 illustrates with boxplots the observed queue joining time of 1000 vehicles for both L-crossing and S/R-crossing lanes at both maximum speeds. The joining times are naturally lower for higher speeds, and so is their variation. There are occasional outliers that correspond to vehicles that find no queue. At lower speeds, the IM policies that generate longer queues also tend to generate shorter joining times.

2) INTERSECTION SERVICE TIME

Once vehicles join the queue, they take the IST to be served by each IM approach. From the FCD data, the observed intersection crossing times are below $4s$ depending on the crossing directions, being shorter for right-crossing.

Figure 11 displays the IST results for both speeds and crossing lanes with different IM approaches showing different distributions. At both maximum speeds and crossing lanes, in all three cases (highest, lowest, and median),
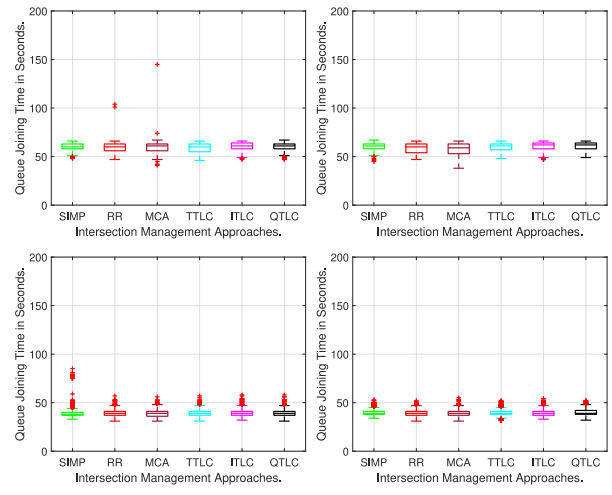

FIGURE 10. Observed queue joining time (s) of 1000 vehicles for $30\,km/h$ (top) and $50\,km/h$ (bottom), L-crossing (left) and S/R-crossing (right) at $\lambda = 0.033\,veh/s$ and $0.067\,veh/s$ respectively, and $C = 50\,veh$.
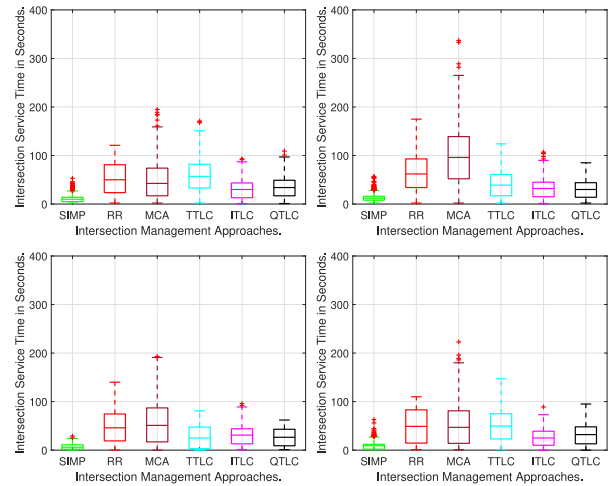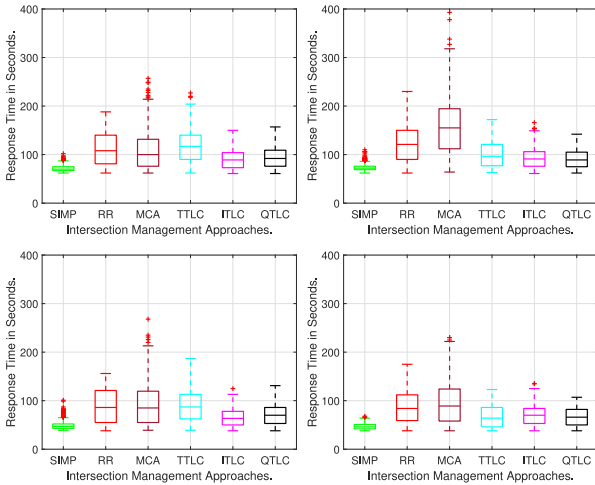

FIGURE 11. Observed intersection service time (s) of 1000 vehicles for $30\,km/h$ (top) and $50\,km/h$ (bottom), L-crossing (left) and S/R-crossing (right) lanes at $\lambda = 0.033\,veh/s$ and $0.067\,veh/s$ respectively, and $C = 50\,veh$.

SIMP is the best performing approach with the lowest IST values. The following best approaches are ITLC and QTLC. Overall, MCA exhibits poor performance due to its working nature, since the green phase circulation is based on the instantaneous traffic flow. Thus, MCA may let vehicles of lanes with instantaneously less traffic wait for more cycles.

3) RESPONSE TIME

As specified earlier, RT is the combination of queue joining time and IST, and their individual results show the highest values that are imposed by the IST and the lowest values are imposed by the queue joining time; and different IM approaches behave differently for both measures. The RT results provide the overall efficiency of IM approaches in non-saturated traffic scenarios. The RT results for both maximum speeds and crossing lanes are presented in Fig. 12. From these results, the following observations can be made.
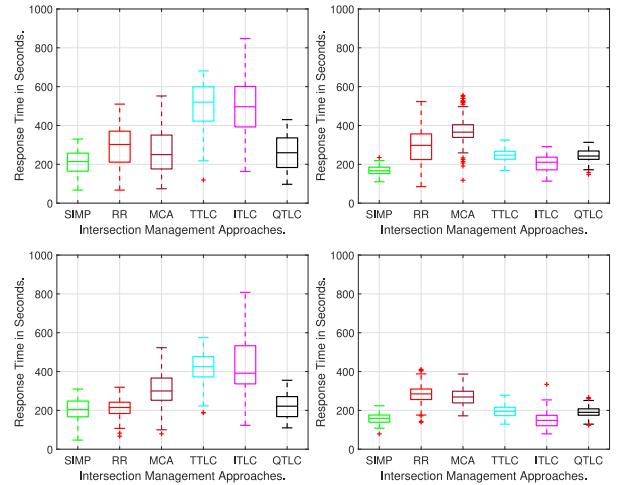
FIGURE 12. Observed response time (s) of 1000 vehicles for 30km/h (top) and 50km/h (bottom), L-crossing (left) and S/R-crossing (right) lanes at $\lambda = 0.033\,veh/s$ and 0.067veh/s respectively, and $C = 50\,veh$ (non-saturated traffic).

FIGURE 13. Observed response time (s) of 50th vehicle for 30km/h (top) and 50km/h (bottom), L-crossing (left) and S/R-crossing (right) lanes at $\alpha(t) = 0.4\,veh/s$ and $C = 50\,veh$ (saturated traffic).

SIMP is the best-performing approach on both crossing lanes and maximum speeds. The following best approaches are the ITLC and QTLC, and their performance order changes from the L-crossing lane to the S/R-crossing lane. Similar behavior can be observed with the RR and TTLC, but it changes with the speed, i.e., from L-crossing 30km/h to S/R-crossing 50km/h and vice versa. In the end, MCA is the poorest-performing IM approach with the highest RT values. When we compare both the L-crossing and S/R-crossing results of MCA, the highest RT values at 30km/h can be noticed in the S/R-crossing lane, while at 50km/h it is in the L-crossing lane.

E. RESPONSE TIME OF SATURATED TRAFFIC FLOW
For analyzing response time during saturated traffic conditions, we ran 100 simulations at a long-term average rate of 0.4veh/s for 1000s. We let the traffic flow during the first 100s to avoid bias caused by initialization and then we analyzed the response time of the 50th vehicle injected after the initial 100s period. We believe the 50th vehicle is close to a worst-case situation, being already unaffected by the initial conditions while the road capacity is not yet flooded in any of the protocols. For this scenario, the traffic generation follows the same pattern as the previous case but with a long-term average arrival rate of $\lambda = 0.4\,veh/s$, divided uniformly among the three crossing directions. Therefore, the S/R-crossing lane accommodates 67% of vehicles at 0.267veh/s, and the L-crossing lane accommodates the remaining 33% of vehicles at 0.133veh/s. The road capacity is also considered to be $C = 50\,veh$. The achieved RT results for the 50th vehicle in all scenarios are presented as boxplots in Figure 13 for L-crossing (left plot) and S/R-crossing (right plot) lanes for 30km/h (above) and 50km/h (below). The highest RT presented serves as the *observed* WCRT.

At 30km/h maximum speed, SIMP shows the lowest RT results for both the maximum and median cases in both S/R- and L-crossing lanes, similar to the non-saturated traffic flow

results. TTLC and ITLC exhibit a significantly higher RT in the L-crossing lanes due to the lower bandwidth they offer to these lanes. Conversely, for S/R-crossing lanes, both RR and MCA show higher RT values. When we increase the maximum speed to 50km/h (lower plots) the RT values generally decrease in all IMs, approximately maintaining their relative behavior. However, in this case, the advantage of SIMP over all other IMs is lost, performing similarly to RR in the L-crossing lanes (left plot) and to ITLC in the S/R-crossing (right plot) lanes.

F. WORST-CASE RESPONSE TIME
Since the WCRT values produced by Eqs. (1) and (2) are higher than those produced by Eqs. (1) and (6), given that Eq. (2) considers whole cycles, we use Eq. (2) for the sake of safety of the analysis.

Figure 14 shows the analytical and observed WCRT values (i.e., the highest RT values) for both 30km/h (above) and 50km/h (below) maximum speeds and L-crossing (left) and S/R-crossing (right) lanes. The first and primary remark is that the observed WCRT values of all IM approaches are below the analytical WCRT values, providing an empirical validation of the WCRT analysis we proposed earlier. Hence, we confirm to some degree of confidence that the analytical WCRT provides upper-bound values to RT, as no empirical observation from the simulations was higher than those values. A second conclusion is that the proposed WCRT analysis offers a level of pessimism that is different for the L-crossing and the S/R-crossing lanes, being particularly low in the second case. Nevertheless, two cases depart from the global pattern, QTLC in L-crossing lanes for both maximum speeds and RR in S/R-crossing lane for 30km/h maximum speed. We believe the pessimism of QTLC emerges from pessimistic assumptions in the analysis that did not capture its adaptation capacity. For RR we believe the pessimism results from a limited simulation time that did not capture worst-case conditions. Removing these outlying cases, on
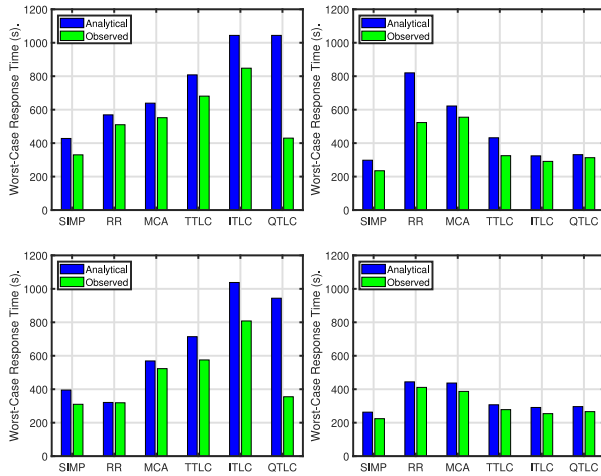
FIGURE 14. Worst-case response time (s) for L-crossing (left) and S/R-crossing (right) lanes at $30km/h$ (top) and $50km/h$ (bottom), $\alpha(t) = 0.4veh/s$, and $C = 50veh$ (saturated traffic).

average the computed WCRTs in saturated conditions were 17.6% ($30km/h$) and 17.95% ($50km/h$) above the observed ones in the L-crossing lanes and 15.3% ($30km/h$) and 11.51% ($50km/h$) in the S/R-crossing lanes.

VII. CONCLUSION

This paper addressed the WCRT of a vehicle (either HV or AV) when crossing a complex intersection operated by an IM protocol in urban scenarios, considering two typical maximum speed settings, namely $30km/h$ and $50km/h$. The traffic was characterized using arrival curves that represent worst-case conditions. We utilized the IM-specific parameters and associated values to draw service curves, including the total control cycle time and the maximum number of vehicles each IM serves in one control cycle. We considered six state-of-the-art IM protocols that manage complex intersections namely SIMP, RR, MCA, TTLC, ITLC, and QTLC. All protocols were implemented in identical geographic conditions using the SUMO simulator.

Our main contribution was an analysis that provides upper bounds for the response time of vehicles crossing the intersection. This analysis was empirically validated using simulations in urban mobility scenarios with both non-saturated and saturated traffic conditions.

A second contribution was the comparison of six IM protocols in terms of their WCRTs, using the analysis and simulations. Among all IMs, SIMP stands out with the lowest WCRTs in all cases. The other protocols present asymmetries between the L-crossing and the S/R-crossing lanes, which are significantly higher under saturated traffic conditions. Under non-saturated traffic, RR, MCA and TTLC reveal the highest WCRT values on both lanes and maximum speeds. However, under saturated conditions, ITLC shows a significant degradation in the L-crossing lanes, with the highest WCRT. In the S/R-crossing lanes, the relative performance is similar for both saturated and non-saturated conditions.

In the future, we will extend this WCRT analysis to a network of homogeneous and heterogeneous intersections during unexpected road events such as emergency vehicle presence, road blockage, and accidents. We will also estimate the saturation speed analytically, employing the appropriate parameters.

DISCLAIMER

This document reflects only the authors' view and the European Commission is not responsible for any use that may be made of the information it contains.

REFERENCES

[1] K. Dresner and P. Stone, "A multiagent approach to autonomous intersection management," *J. Artif. Intell. Res.*, vol. 31, pp. 591–656, Mar. 2008.

[2] M. B. Younes and A. Boukerche, "An intelligent traffic light scheduling algorithm through vanets," in *Proc. 39th Ann. IEEE Conf. Local Comput. Netw. Workshops*, 2014, pp. 637–642.

[3] M. Khayatian, Y. Lou, M. Mehrabian, and A. Shirvastava, "Crossroads+: A time-aware approach for intersection management of connected autonomous vehicles," *ACM Trans. Cyber-Phys. Syst.*, vol. 4, no. 2, pp. 1–28, Nov. 2019.

[4] M. Khayatian, R. Dedinsky, S. Choudhary, M. Mehrabian, and A. Shrivastava, "R 2 IM-robust and resilient intersection management of connected autonomous vehicles," in *Proc. IEEE 23rd Int. Conf. Intell. Transp. Syst. (ITSC)*, 2020, pp. 1–6.

[5] M. Khayatian et al., "A survey on intersection management of connected autonomous vehicles," *ACM Trans. Cyber-Phys. Syst.*, vol. 4, no. 4, pp. 1–27, 2020.

[6] R. Chen, J. Hu, M. W. Levin, and D. Rey, "Stability-based analysis of autonomous intersection management with pedestrians," *Transp. Res. C, Emerg. Technol.*, vol. 114, pp. 463–483, May 2020.

[7] P. Bansal and K. M. Kockelman, "Forecasting Americans' long-term adoption of connected and autonomous vehicle technologies," *Transp. Res. A, Policy Pract.*, vol. 95, pp. 49–63, Jan. 2017.

[8] G. Sharon and P. Stone, "A protocol for mixed autonomous and human-operated vehicles at intersections," in *Proc. Int. Conf. Auton. Agents Multiagent Syst.*, 2017, pp. 151–167.

[9] R. Reddy, L. Almeida, and E. Tovar, "Work-in-progress: Synchronous intersection management protocol for mixed traffic flows," in *Proc. IEEE Real-Time Syst. Symp. (RTSS)*, 2019, pp. 576–579.

[10] R. Reddy, L. Almeida, P. M. Santos, and E. Tovar, "Comparing the ecological footprint of intersection management protocols for human/autonomous scenarios," in *Proc. IEEE 23rd Int. Conf. Intell. Transp. Syst. (ITSC)*, 2020, pp. 1–6.

[11] I. Mahdinia, A. Mohammadnazar, R. Arvin, and A. J. Khattak, "Integration of automated vehicles in mixed traffic: Evaluating changes in performance of following human-driven vehicles," *Accid. Anal. Prev.*, vol. 152, Mar. 2021, Art. no. 106006.

[12] P. Oza and T. Chantem, "A real-time server based approach for safe and timely intersection crossings," in *Proc. IEEE 25th Int. Conf. Embed. Real-Time Comput. Syst. Appl. (RTCSA)*, 2019, pp. 1–12.

[13] P. Oza, T. Chantem, and P. Murray-Tuite, "A coordinated spillback-aware traffic optimization and recovery at multiple intersections," in *Proc. IEEE 26th Int. Conf. Embed. Real-Time Comput. Syst. Appl. (RTCSA)*, 2020, pp. 1–10.

[14] P. Oza and T. Chantem, "Timely and non-disruptive response of emergency vehicles: A real-time approach," in *Proc. 29th Int. Conf. Real-Time Netw. Syst.*, 2021, pp. 192–203.

[15] R. Reddy, L. Almeida, M. Gaitan, H. Kurunathan, P. Santos, and E. Tovar, "Work-in-progress: Worst-case response time of intersection management protocols," in *Proc. IEEE Real-Time Syst. Symp. (RTSS)*, 2021, pp. 556–559.

[16] L. Miao and D. Leitner, "Adaptive traffic light control with quality-of-service provisioning for connected and automated vehicles at isolated intersections," *IEEE Access*, vol. 9, pp. 39897–39909, 2021.

[17] A. Ghosh and T. Parisini, "Traffic control in a mixed autonomy scenario at urban intersections: An optimal control approach," *IEEE Trans. Intell. Transp. Syst.*, vol. 23, no. 10, pp. 17325–17341, Oct. 2022.

[18] P. A. Lopez et al., "Microscopic traffic simulation using SUMO," in *Proc. 21st Int. Conf. Intell. Transp. Syst. (ITSC)*, 2018, pp. 2575–2582.

[19] H. Chaudhuri, V. Masti, V. Veerendranath, and S. Natarajan, "A comparative study of algorithms for intelligent traffic signal control," in *Proc. Mach. Learn. Auton. Syst. (ICMLAS)*, 2022, pp. 271–287.

[20] E. Björck and F. Omstedt, *A Comparison of Algorithms used in Traffic Control Systems*, KTH Royal Inst. Technol., Stockholm, Sweden, 2018.

[21] P. Varaiya, "Max pressure control of a network of signalized intersections," *Transp. Res. C, Emerg. Technol.*, vol. 36, pp. 177–195, Nov. 2013.

[22] S. A. Ramadhan, H. Y. Sutarto, G. S. Kuswana, and E. Joelianto, "Application of area traffic control using the max-pressure algorithm," *Transp. Plan. Tech.*, vol. 43, no. 8, pp. 783–802, 2020.

[23] B. Abdulhai, R. Pringle, and G. J. Karakoulas, "Reinforcement learning for true adaptive traffic signal control," *J. Transp. Eng.*, vol. 129, no. 3, pp. 278–285, 2003.

[24] R. Reddy, L. Almeida, M. G. Gaitán, P. M. Santos, and E. Tovar, "Synchronous framework extended for complex intersections," in *Proc. 24th Euro Work. Group Transp. Meet.*, 2021, pp. 1–3.

[25] X. Liu, P.-C. Hsieh, and P. R. Kumar, "Safe intersection management for mixed transportation systems with human-driven and autonomous vehicles," in *Proc. 56th Annu. Allerton Conf. Commun., Control, Comput. (Allerton)*, 2018, pp. 834–841.

[26] R. Reddy, L. Almeida, P. M. Santos, S. Bouzefrane, and E. Tovar, "Synchronous intersection management to reduce time loss," *Transp. Res. Proc.*, vol. 52, pp. 364–372, Jan. 2021.

[27] L. A. Rodegerdts et al., *Signalized Intersections: Informational Guide*, Federal Highway Admin. Gov. Agency, Washington, DC, USA, 2004.

[28] L. Alekszejenkó and T. P. Dobrowiecki, "Sumo based platform for cooperative intelligent automotive agents," in *Proc. SUMO Conf.*, 2019, pp. 107–123.

[29] R. Reddy, L. Almeida, P. Santos, and E. Tovar, "Waiting time analysis for a network of signalized intersections," *Procedia Comput. Sci.*, vol. 220, pp. 503–510, Jan. 2023.

[30] H. C. Manual, *A Guide for Multimodal Mobility Analysis*, Transp. Res. Board, Washington, DC, USA, 2016.

[31] Y. Ş. Murat and M. Cetin, "A new perspective for saturation flows at signalized intersections," *Periodica Polytechnica Civil Eng.*, vol. vol. 63, no. 1, pp. 296–307, 2019.

[32] C. Daganzo and G. Newell, *Methods of Analysis for Transportation Operations*, Inst. Transp. Studies, Univ. California Berkeley, Berkeley, CA, USA, 1995.

[33] S. Krauß, *Microscopic Modeling of Traffic Flow: Investigation of Collision Free Vehicle Dynamics*, Universität zu Kööln, Cologne, Germany, 1998.

[34] V. Milanés and S. E. Shladover, "Modeling cooperative and autonomous adaptive cruise control dynamic responses using experimental data," *Transp. Res. C, Emerg. Technol.*, vol. 48, pp. 285–300, Nov. 2014.

[35] E. Matsoukis and S. Efstathiadis, "An investigation of the variability of start-up lost times and departure headways at signalized intersections in urban areas," in *Urban Transport XVI: Urban Transport and the Environment in the 21st Century*, vol. 111, Southampton, U.K.: Wit press, 2010, p. 59.

LUIS ALMEIDA (Senior Member, IEEE) graduated from the University of Aveiro, Portugal.

He is currently an Associate Professor with the Electrical and Computer Engineering Department, University of Porto, Portugal, where he coordinates the Distributed and Real-time Embedded Systems Laboratory. He is also the Vice-Director of the CISTER Research Center on Real-Time and Embedded Computing Systems. His main interests include real-time communications for distributed industrial/embedded systems, for teams of cooperating agents, and for sensor networks. He is the Past Chair of the IEEE Technical Committee on Real-Time Systems (Chair in 2020–2021) and the Chair of the EDAA Special Interest Group on Embedded Systems. He is an Editor-in-Chief of the *Real-Time Systems* (Springer) and an Associate Editor of the *Journal of Systems Architecture* (Elsevier) and the *International Journal on Advanced Robotic Systems* (SAGE). He was the Program and General Chair of the IEEE Real-Time Systems Symposium in 2011 and 2012, respectively, and the Local Co-Chair in 2016, as well as the General Co-Chair of CPSweek 2018. He was also a Trustee of the RoboCup Federation from 2008 to 2016 and the Vice-President from 2011 to 2013.

HARRISON KURUNATHAN received the bachelor's degree in the field of electronics and communication from SRM University in 2012, the master's degree in very large-scale integration from the SSN College of Engineering, Anna University in 2014, and the Ph.D. degree in electrical and computer engineering from the University of Porto, Portugal, in 2021.

He joined the CISTER Research Centre in 2014 to work in the domain of Wireless Sensor Networks. Since then, he has been working in areas, such as improving quality of service for industrial and low-rate WSN infrastructures, and network protocols. During his tenure as a Ph.D. student, he was actively involved in the SafeCOP Project that aims toward safety-related Cooperating cyber-physical systems. He has several publications in reputed conferences (e.g., WFCS, ICCPS, RTN) and journals (e.g., IEEE COMMUNICATION SURVEYS AND TUTORIALS and IEEE ACCESS).

Dr. Kurunathan has served as a reviewer for several conferences (e.g., ICCPS, EWSN, MSN, RTN) and journals (e.g., IEEE ACCESS, IEEE TRANSACTIONS ON VEHICULAR TECHNOLOGY, and *ACM Sigbed*).

RADHA REDDY (Member, IEEE) received the B.Sc. and M.Sc. degrees in computer science from Sri Venkateswara University in 2007 and 2009, respectively, the M.Tech. degree in computer science and engineering from JNTU-Anantapur in 2014, and the Ph.D. degree (FCT Fellowship in 2021) in electrical and computer engineering from the Faculty of Engineering, University of Porto in 2023.

He is currently an Assistant Professor of Computer Science and Engineering with the Amrita School of Computing, Amrita Vishwa Vidyapeetham, India. Since October 2013, he has been an External Collaborator with the CEDRIC Labs, CNAM-Paris, France. He is also a Research Collaborator with the CISTER Research Center (ISEP). Before the CISTER Research Center, he was involved in full-time research with COPELABS-Lisbon and Inria-Paris. His research interests include intelligent transportation systems, multi-agent systems, cyber–physical systems, self-organized systems, and the coordination and cooperation of heterogeneous networked systems.

MIGUEL GUTIÉRREZ GAITÁN (Senior Member, IEEE) received the B.Sc. degree in electronics engineering from the Pontifical Catholic University of Valparaiso, Chile, in 2007, the M.Sc. degree in telecommunications engineering from the Polytechnic University of Turin, Italy, in 2009, and the Ph.D. degree in electrical and computer engineering from the University of Porto, Portugal, in 2023. He is an Assistant Professor with the Department of Electrical Engineering, Pontifical Catholic University of Chile, Chile. He serves as a Research Collaborator of the Research Centre in Real-Time and Embedded Computing Systems, Portugal. His research focuses on wireless networks, real-time communication, and Internet of Things. He currently chairs the IEEE ComSoc Chile Chapter in 2023–2024.

PEDRO M. SANTOS received the B.Sc. and M.Sc. degrees in electrical and computer engineering from the University of Porto, Portugal, in 2009, and the Ph.D. degree in electrical and computer engineering from the University of Porto in 2017, in collaboration with the Instituto de Telecomunicações (Portuguese R&D Institution). He currently holds positions as an Assistant Researcher with the CISTER Research Unit, Porto, Portugal, and as an invited Assistant Lecturer with the University of Porto. He has been a P.I. for international projects, notably Eureka ITEA3 "MIRAI" and Carnegie Mellon University-Portugal Program "FLOYD." Prior, he was a Postdoctoral Fellow and the Ph.D. student researcher in numerous Portuguese (P2020), European (FP7), and international projects (CMU-Portugal program). He was a Visitor to Carnegie Mellon University for three months. His research interests are in wireless propagation, 5G/6G, vehicular networking, and Internet of Things for smart cities. He has published and is a reviewer for a number of forums on communications and networking (IEEE TWC, VNC, VTC), and served or serves as a TPC member for IEEE VNC, WCFS, and EAI Future5V.

EDUARDO TOVAR (Member, IEEE) received the Licentiate, M.Sc., and Ph.D. degrees in electrical and computer engineering from the University of Porto, Porto, Portugal, in 1990, 1995, and 1999, respectively. He is currently a Professor with the Computer Engineering Department, School of Engineering (ISEP), Polytechnic Institute of Porto, where he is also engaged in research on real-time distributed systems, WSN, multiprocessor systems, CPS, and industrial communication systems. He heads the CISTER Research Labs. Since 1991, he authored or coauthored more than 300 scientific papers in the areas of RTES, CPS, and WSN. He has consistently participated in top-rated scientific events as Program Chair (e.g., ECRTS-2005, RTCSA-2010 and 2016, RTAS-2013, ICCPS-2016). He was the Vice-Chair of ACM SIGBED from 2015 to 2019 and a member of the Executive Committee of the IEEE TC-RTS. He has been general chair/co-chair of various scientific events, including the IEEE/ACM CPS Week 2018.